Spatio-temporal differences in presentation of CD8 T cell epitopes during HBV infection.

Atefeh Khakpoor[1], Yi Ni[2,3], Antony Chen[4], Zi Zong Ho[5], Vincent Oei[1], Ninghan Yang[6], Reshmi Giri[1] , Jia Xin Chow[1], Anthony T. Tan[1], Patrick T.Kennedy[8], Mala Maini[7], Stephan Urban[2,3], Antonio Bertoletti[1,6*].

[1]*Emerging Infectious Diseases Program, Duke-NUS Medical School, Singapore;*

[2]*Department of Infectious Diseases, Molecular Virology, University Hospital Heidelberg, Heidelberg, Baden-Württemberg, Germany*

[3]*German Center for Infection Research (DZIF), partner site Heidelberg, Heidelberg, Germany*

[4]*Infectious Disease & Vaccines, Janssen Pharmaceuticals, Beerse, Belgium*

[5]*Lion TCR Private Limited, Singapore*

[6]*Singapore Immunology Network, A*STAR, Singapore*

[7]*Division of Infection and Immunity, University College London, London, United Kingdom*

[8] *Hepatology, Centre for Immunobiology, Blizard Institute, Barts and The London School of Medicine & Dentistry, QMUL, London, United Kingdom*

Running Title: Hepatic distribution of HLA-class I /HBV peptide complexes.

Corresponding Author:

Antonio Bertoletti

Emerging Infectious Diseases

Duke-NUS Medical School

8 College Road, Singapore 169857.

Phone: +65 6601137 Email: antonio@duke-nus.edu.sg

Abstract

Distinct populations of hepatocytes infected with HBV or only harboring HBV-DNA integrations coexist within an HBV chronically infected liver. These hepatocytes express HBV antigens at different levels and with different intracellular localizations but it is not known whether this heterogeneity of viral antigen expression could result in an uneven hepatic presentation of distinct HBV epitopes/HLA class-I complexes triggering different level of activation of HBV-specific CD8+ T cells.

Using antibodies specific to two distinct HLA–A*02:01/HBV epitope complexes of HBV nucleocapsid and envelope proteins, we mapped their topological distribution in liver biopsies of two anti-HBe+ chronic HBV (CHB) patients. We demonstrated that the core and envelope CD8+T cell epitopes were not uniformly distributed in the liver parenchyma but preferentially located in distinct and sometimes mutually exclusive hepatic zones. The efficiency of HBV epitope presentation was then tested *in vitro* utilizing HLA-A*02:01/HBV epitope-specific antibodies and the corresponding CD8+ T cells, in primary human hepatocyte and hepatoma cell lines either infected with HBV or harboring HBV-DNA integration. We confirmed the existence of a marked variability in the efficiency of HLA-class I/HBV epitope presentation among the different targets that was influenced by presence of IFN-γ and availability of newly-translated viral antigens. In conclusion, HBV antigen presentation can be heterogeneous within an HBV-infected liver. As a consequence, CD8+ T cells of different HBV specificities might have different antiviral efficacy.

Importance

The inability of patients with chronic HBV infection to clear HBV is associated with defective HBV-specific CD8+ T cells. Hence, the majority of immunotherapy developments focus on HBV specific T cell function restoration. However, knowledge of whether distinct HBV-specific T cells can equally target all the HBV-infected hepatocytes of a chronically infected liver are lacking. In this work, analysis of CHB patient liver parenchyma and *in vitro* HBV infection models shows a non-uniform distribution of HBV CD8+ T cells epitopes that is influenced by presence of IFN-γ and availability of newly-translated viral antigens. These results suggest that CD8+ T cells recognizing different HBV epitopes can be necessary for efficient immune therapeutic control of chronic HBV infection.

Introduction

CD8+ T cells play an important role in protecting the host against viral infections. Using their specific T cell receptors (TCR), CD8+ T cells recognize and subsequently lyse virus-infected cells expressing HLA class-I/viral peptide complexes on their surface (1). The efficiency of HLA class-I/viral peptide complex formation is essential for the recognition of virus-infected cells by CD8+ T cells (2); viruses that can establish chronic infection such as HCMV and HIV have evolved strategies to modulate either processing or presentation of these complexes (3).

The ability of CD8+ T cells to recognize HBV-infected hepatocytes has been studied in chimpanzees (4) and humanized chimeric mouse models (5). However, due to the technical difficulties in establishing HBV infection in primary human hepatocyte (PHH) *in vitro* (6), the efficiency of HBV epitope presentation after infection has never been analyzed in details. Most studies on CD8+ T cell recognition of HBV-infected targets employed experimental systems in which HBV antigen expression was driven by either viral vector transfections (EBO, Vaccinia, Adeno)(7-9) or HBV-DNA integration into the host genome (HepG2.2.15 or HBV transgenic mice)(10-12). Only following the recent characterization of the HBV entry receptor human sodium taurocholate co-transporting polypeptide (hNTCP) (13), a robust HBV infection system has been established in HepG2-hNTCP-A3 cells (14) allowing the study of human HBV core-specific CD8+ T cell recognition of HBV-infected targets *in vitro* (15). However, whether distinctive epitopes originating from different HBV proteins are differently presented during infection is not known. Equally, the ability of HepG2-hNTCP-A3 to process and present viral antigens may differ from that of normal hepatocytes since defects in antigen presentation have been suggested to occur in HCC cells(16).

Similarly, although HLA class-I/HBV peptide complexes can be directly visualized on

liver biopsies of chronically infected patients (17, 18), knowledge related to the efficiency and kinetics of the generation of HLA class-I/HBV peptide complexes in CHB infected livers is limited (19, 20). Studies investigating the localization of HBV-infected hepatocytes in the liver of patients with chronic hepatitis B showed a complex mosaic of cells expressing HBV antigens at different levels and localizations (21, 22) and with broad differences in the ratio between HBsAg and cccDNA levels (23-25). This differential antigenic expression is likely caused by the concomitant presence of hepatocytes infected with HBV for different durations and/or the production of HBV antigens from either integrated HBV-DNA or cccDNA (25 26).

Overall, whether HBV-specific CD8+ T cells are able to distinguish distinct populations of HBV antigen-expressing hepatocytes is unknown. Investigations of HBV-specific T cells during natural infection have focused exclusively on their quantity (7, 27, 28), function (29) and localization (28, 30), whilst the ability of hepatocytes to present HBV epitopes to their cognate HBV-specific CD8+T cells has been neglected. To fill this knowledge gap, we first utilized T cell receptor like antibodies (TCRL-Ab) specific for two distinct HBV epitopes derived from envelope and nucleocapsid antigen and presented by HLA-A*02:01 to analyze their distribution in the liver of CHB patients.

We then compared the *in vitro* efficiency of presentation of different HLA class-I/HBV epitopes in HBV-infected PHH and in hepatocyte-like cell lines (HepG2-hNTCP-A3, HepG2.2.15, HepG2-Env, PLC/PRF5/HLA-A2+) infected by HBV or expressing HBV antigens from HBV-DNA integration. We demonstrated that distinct epitopes are presented with differing efficiency and that the presence of IFN-γ and availability of newly-translated viral antigens modulate the quantity of HBV epitope presentation.

Results

Heterogeneous distribution of CD8+ T cell core and envelope epitopes in chronic HBV-infected human liver

We first performed a comparative analysis of the distribution of two HBV epitope/HLA class-I complexes within HBV-infected livers. We utilized antibodies that have been already demonstrated to specifically recognize respectively the HLA-A*02:01/HBc18-27 (defined as Ab A2-HBc18) and the HLA-A*02:01/HBs183-191 (defined as Ab A2-HBs183) complexes in HBV-infected cells and in biopsies of HLA-A*0201^{+} patients with CHB (17, 18).

Liver biopsies of 8 HLA-A*0201^{+} CHB patients (Table 1) were stained with above mentioned antibodies and analyzed with TissueFAXS immunofluorescent microscopy to create high-resolution images of whole biopsies. Note that, since both Ab A2-HBc18and Ab A2-HBs183 antibodies are raised in mouse and not directly conjugated with fluorochrome, this comparative analysis of the different localization of the A2-HBc18 and A2-HBs183 complexes had to be done by staining individual tissue slides corresponding to two consecutive sections. Table 1 shows that only 3 out of 8 HLA-A*02:01^{+} liver biopsies showed positive staining. Interestingly, all 3 positive biopsies are CHB patients of Caucasian ethnicity and infected with genotype D (Fig1a -d), while 5 of negative biopsies derived from CHB patients of Chinese ethnicity infected with genotype B and C (Fig 1e). This is likely to be caused by the natural amino acid substitutions present within the HBc18-27 and HBs183-91 sequences present in HBV genotype B and C while both antibodies were raised utilizing epitopes sequences of HBV genotype D (31).

The staining of the two antibodies was not uniformly distributed among the hepatic parenchyma but varied in intensity and localization. Figure 1a and c show a representative image of two anti-HBe+ CHB patients. A2-HBc18 and A2-HBs183

complexes were visualized only in the hepatic parenchyma (Fig 1a, c) and not in the fibrotic portal tracts (Fig 1a,c), further confirming the specificity of our antibodies. Furthermore, not only was there a non-uniform distribution of both epitopes within the hepatic tissue, but the two different HLA-class I/HBV-epitopes can be detected in distinct anatomical regions. For example, in region B (schematic in Fig1a), there was a robust detection of A2-HBc18 complexes, whereas A2-HBs183 complex detection was negligible (Fig 1a). On the other hand, region C had a predominant expression of A2-HBs183 complexes with low or absent A2-HBc18 complex detection (Fig 1a). Analysis of HBV antigens (HBcAg and HBsAg) expression was performed in these two CHB patients. Figure1 b and d show that the region of higher A2-HBs183 complex detection were topologically correlated with HBsAg expression. Unfortunately, technical problems hamper a detection of HBcAg localization in these two biopsies preventing the parallel analysis of A2-HBc18 and HBcAg expression.

Finally, detection of these two HLA-A*02:01/HBV epitopes was completely negative in other hepatic parenchymal regions (Region D). Similar results were observed in the biopsy of second CHB patient (anti-HBe+) which stained positive with both antibodies (Fig 1c and d). Therefore, this analysis shows that at least in anti-HBe+ CHB patients expression of distinct HBV epitopes have a mosaic pattern of distribution.

Establishing an *in vitro* system of HBV infection

In order to study the regulation of HBV derived epitope presentation in a more controlled *in vitro* system, we established an infection system to mimic acute HBV infection (arbitrarily defined as events occurring 12hrs to 7 days post-infection (p.i)) using PHH and HepG2-hNTCP-A3 (Fig 2a) The HLA-class I compatibility between target and our reagents (HLA-A*02:01-restricted HBc18-27 and HBs183-91-specific CD8+ T cell clones and the two TCR-like antibodies (Ab A2-HBc18 and Ab-A2-HBs183) was retained by

using HLA-A*02:01+ PHH while HepG2-hNTCP-A3 cells are HLA-A*02:01+. Both PHH and HepG2-hNTCP-A3 cells were infected at multiplicities of genome equivalent (GEV) of 3000/cell, as shown in schematic (Fig 2a). Establishment of productive HBV replication upon infection was confirmed by measuring HBV 3.5 Kb mRNA (pre-genomic RNA/pgRNA) using nanostring technology while expression of HBcAg and HBsAg was quantified by flow cytometry using anti-HBs and anti-HBc specific antibodies at 12 hours, 18 hours, days 1, 3 and 7 p.i Nanostring probe design is shown in figure 2b.The specificity of probes (results related to HBV S mRNA and HBV 3.5 kb mRNA is shown) is tested in cells overexpressing individual HBV peptide (HepG2-Env) or harboring full HBV genome integration (HepG2.2.15), as shown in figure 2c and d.

In both PHH and HepG2-hNTCP-A3 cells (Fig 2e), pre-genomic RNA was already detectable at 18 hours p.i and progressively increased until day 7. HBcAg and HBsAg detection also increased gradually from 18 hours to day 7 p.i in both PHH and HepG2-hNTCP-A3 cells. The frequency of positive cells for HBV antigens in HBV-infected cells was higher in hepatocytes (> 60% positive cells for HBV antigens at day 3 p.i, Fig 2f) than HepG2-hNTCP-A3 (~ 40 to 50 % at day 7 p.i, Figure 2f). Interestingly, the frequency of HBsAg expressing hepatocytes was slightly higher than that of core expressing ones, while this trend was opposite in HBV-infected HepG2-hNTCP-A3.

Having established two *in vitro* HBV infection systems, we analyzed the hierarchy of HBV epitope presentation in both HBV-infected hepatocytes and HepG2-hNTCP-A3 (schematic figure 3a). First, we tested whether the level of HLA-class I expression was modified by HBV infection. In line with different evidence showing that HBV can replicate within hepatocytes without being sensed by innate immunity sensors (32), we did not detect variations either in HLA-class I mRNA (data not shown) or protein expression upon infection in both systems (Fig 2g).

We then analyzed the surface expression of HLA-A*02:01/HBV epitopes complexes. HBV-infected hepatocytes and HepG2-hNTCP-A3 cells were stained with anti-HBcAg antibodies and with the two TCR-like antibodies (17) over the duration of infection. The expression of two HBV epitopes was analyzed after gating on cells which were productively synthesizing HBcAg (gating strategy shown in Fig 3b). The quantity of the core and envelope derived epitopes did not increase in HBcAg-expressing targets over time. However, the presentation of both core and envelope epitopes was more efficient in PHH than HepG2-hNTCP-A3 and the A2-HBc18 complexes were presented more efficiently than the A2-HBs183 complexes both in hepatocytes and HepG2-hNTCP-A3. In contrast to peptide-pulsed targets (HepG2-pulsed with 1uM of peptide),the surface distribution of the HLA/HBV epitope complex on HBV-infected HepG2-hNTCP-A3 cells was in discrete cluster (Figure 3c).

We then tested the ability of HBc18-27 and HBs183-91 specific CD8+ T cells to recognize HBV-infected targets. By day 1 after HBV infection hepatocytes activated both HBc18-27 and HBs183-91 specific CD8+ T cells (Fig 3d) . CD8+T cell activation (tested as CD107a and IFN-γ/TNF-α expression -Fig 3d) progressively increased from day 1 to day 7, as a likely result of the increased quantity of hepatocytes expressing the two different epitopes. Furthermore, HBs183-91 CD8+ T cells were activated more efficiently by PHH than HepG2-hNTCP-A3 infected cells (Fig 3d) in line with the superior presentation ability of PHH detected by TCR-like antibody staining.

Effect of IFN-γ on HBV CD8+ T cell epitope presentation

Efficient generation of viral epitopes in infected cells can be modulated by the presence of cytokines and particularly by IFN-γ, which is known to activate cellular immunoproteasomes(33). We tested the effect of IFN-γ treatment (at 100IU/ml for 48 hours) on HBV-infected hepatocytes and HepG2-hNTCP-A3 (schematic figure 4a). As

212 expected (33), IFN-γ treatment increased the surface expression of HLA-class I
213 molecules, as well as the mRNA expression level of the immunoproteasome subunit,
214 *PSMB8 and PSMB9* (data not shown).
215 We then directly measured the quantity of HLA-A*02:01/HBV epitope complexes with
216 TCR-like antibodies in HBcAg + and HBcAg- populations of infected targets (Figure 4b).
217 Note that treatment of IFN-γ didn't have any effect on TCR-like antibody staining in
218 HBcAg negative population in comparison with HBcAg+ population of the infected
219 targets (Fig 4c). In contrast, in HBcAg+ populations, IFN-γ treatment increased the
220 surface expression of A2-HBs183 complexes at all time points but it has a more limited
221 effect on A2-HBc18 expression (Fig 4b). We then tested the impact of IFN-γ treatment
222 on HBc18-27 and HBs183-91 specific CD8+ T cell recognition of infected targets. IFN-γ
223 treatment did not alter HBc18-27-specific CD8+ T cell activation (Fig4d, left panels) but
224 significantly increased HBs183-91-specific CD8+ T cell activation (Fig 4d, right panels)
225 (shown as CD107a+ CD8+ T cells), as early as day 1 post infection, with approximately
226 >40% of activated HBs183-91 CD8+ T cells detected by day 7 post-infection (Fig 4d,
227 right panels). Activation of CD8+T cells measured by IFN-γ production displayed a
228 similar pattern (data not shown). Thus, the presence of inflammatory cytokines (IFN-γ)
229 affects epitope presentation in HBV-infected cells.
230 **HBV-epitope/HLA-A*02:01 complex presentation requires NTCP-mediated HBV**
231 **internalization and synthesis of viral proteins**
232 It was previously shown that HBsAg can be efficiently cross-presented by dendritic cells
233 and monocytes treated with inflammatory cytokines (34). Since HBV infection of PHH
234 and HepG2-hNTCP-A3 cells was performed utilizing a high dose of virus (GEV of
235 3000/cell), we sought to determine if HBV antigen presentation by HLA-Class I
236 molecules was the result of cross-presentation of exogenous viral antigens or

processing of endogenously synthesized antigen. Both PHH and HepG2-hNTCP-A3 were infected with HBV either in the presence or absence of the viral entry inhibitor Myrcludex–B peptide (800 nM) with or without IFN-γ treatment (Figure 5a). In both infection systems HBs183-91 and HBc18-27-specific CD8+ T cell activation was significantly reduced (Fig 5b).

Furthermore, HBV infection was carried out with UV inactivated virus. Due to limited number of PHH, this experiment was performed only with HepG2-hNTCP-A3. Regardless of IFN-γ treatment, HBs183-91 and HBc18-27-specific CD8+ T cell activation was significantly reduced in UV inactivated HBV-infected targets (Fig 5c). Thus, these results show that the generation of HBs183-91 and HBc18-27 epitope is not the result of cross-presentation of HBV proteins present in initial HBV inoculum. At the contrary, since both MyrB (Fig 5d) and UV inactivation (data not shown) suppress the HBV antigen expression, epitopes presentation requires HBV entry and synthesis of viral proteins. Note that experiments performed with HBV infected HepG2-hNTCP-A3 treated with nucleoside analogue (NA)(Lamivudine, 10µM) didn't suppress HBV epitope presentation (Fig 5e) since NA blocks HBV DNA and not protein synthesis.

CD8+ T cell recognition of targets with HBV-DNA integration

A variable quantity of hepatocytes present in chronically infected livers are not HBV-infected but carry HBV-DNA integrations and this phenomenon is more intense in anti-HBe+ patients(23, 25, 26). We analyzed the HLA class-I /HBV epitope complex expression on target cells with HBV-DNA integration: HepG2.2.15 (HepG2 cells with full HBV genome integration) (10), HepG2-Env (HepG2 cells with full HBV genotype D envelope) (35) and PLC/PRF5/HLA-A2+ (natural HCC line with partial HBV surface antigen DNA integration (36) transduced with the HLA-A*02:01 molecule).

All cell lines produced HBsAg constitutively and showed a higher expression of A2-

HBs183 complexes compared to HBV-infected HepG2-hNTCP-A3 at day 7 post-infection (Fig 6a). The quantity of complexes was higher than what was observed in infected HepG2-hNTCP-A3 in the presence of IFN-γ. Furthermore, cells with full HBV genome integration (HepG2.2.15) could present A2-HBc18 complexes at a higher level than that quantified in HBV-infected HepG2-hNTCP-A3, regardless of the presence of IFN-γ (Fig 6b).

Moreover, these cells could activate HBs183-91 CD8+ T cells as efficiently as, or even better than HepG2-hNTCP-A3-infected targets in the presence of IFN-γ (Fig 6c). Since viral epitopes should be derived preferentially from newly synthetized proteins, we analyzed whether the increased quantity of HBV epitopes derived from the protein coded by integrated HBV DNA were proportional to the level of mRNA. We quantified HBV large S mRNA expression levels in the cell lines containing HBV-DNA integration in comparison with acutely-infected HepG2-hNTCP-A3 targets. The level of HBs mRNA in cells with HBV-DNA integration was higher (Fig 6d). Taken together, these data show that at least in HepG2 derived lines, HBV epitopes are presented in higher quantities in targets producing antigens from HBV-DNA integration. The epitope presentation is proportional to the quantity of HBV antigen mRNA detected in the different targets suggesting that the quantity of newly synthetized proteins might regulate the efficient presentation of HBV peptides

Differential final intracellular distribution of HBV antigens does not alter HBV epitope presentation

HepG2-hNTCP-A3 lines could be maintained *in vitro* for prolonged periods (up to 28-30 days after HBV infection). We used confocal laser scanning microscopy to evaluate the cellular localization of HBcAg and HBsAg over the duration of infection.

HBsAg showed a diffuse cytoplasmic and/or membranous pattern irrespective of length

of infection (Fig 7a). In contrast, HBcAg displayed a predominantly cytoplasmic distribution during early phases of infection (days 7 and 14), whilst during prolonged infection (days 21 and 28) its localization was increased in the nucleus. This variable intracellular localization has also been observed in the liver of patients with chronic HBV infection and has been hypothesized to regulate HBV-specific T cell recognition (Fig 7b) (21, 22). Thus, we determine whether the final localization of core antigen (from cytoplasm to nucleus) in HBV-infected HepG2-hNTCP-A3 (Fig 7b) might alter the efficiency of HBV antigen presentation. No difference in the quantity of A2-HBc18 complexes or the activation of HBc18-27 specific CD8+ T cells was observed at days 7, 14, 21 and 28 post HBV infection in HepG2-hNTCP-A3 (Fig 7c and 7d). Thus, these data show that the final different intracellular localizations of core antigen do not alter the processing and presentation of the HBc18-27 epitope.

Discussion

The HBV-infected liver contains a mosaic of hepatocytes expressing HBV antigens in different quantities, localizations (23-25) and from different sources (cccDNA or HBV-DNA integration) (26). Here, we analyzed, to our knowledge for the first time, not the distribution of HBV proteins but the one of HLA class-I/HBV peptide complexes within the hepatic parenchyma. Even though our analysis is restricted to only two anti-HBe+ CHB patients we directly observed that HLA class-I/HBV epitopes can be not equally distributed in the liver but , at the contrary, preferentially present in distinct and sometimes mutually exclusive hepatic zones.

We then analyzed the possible causes of this target heterogeneity in HBV-infected PHH and hepatoma cell lines either infected with HBV (HepG2-hNTCP-A3) or with HBV-DNA integration (HepG2.2.15, HepG2-Env and PLC/PRF5-A2+). By using HBV-specific

CD8+ T cells and antibodies specific to HLA class-I/HBV peptide complexes, we demonstrated that presentation efficiency of different HLA-class I restricted HBV epitopes is modulated by the presence of IFN-γ and by the level of production of newly translated antigens.

These findings might have important consequences for the design of immunotherapies targeting HBV chronically infected liver since CD8+ T cells of different HBV epitope specificities would not have an identical capacity to recognize the heterogeneous population of HBV-infected hepatocytes.

Furthermore, by comparing the ability of cells in expressing HBV antigens from infection (PHH and HepG2-hNTCP-A3) and from integration (HepG2.2.15, HepG2-Env and PLC/PRF5-A2+), we showed that the HLA-A*02:01 immunodominant HBs183-91 envelope epitope (37) was presented more efficiently in targets with HBV-DNA integration than in HBV infected HepG2-hNTCP-A3. Future studies need to be performed to understand whether the differences can be generalized to normal HBV infected hepatocytes with HBV-DNA integration

These finding depicts a scenario where hepatocytes with HBV-DNA integration, could act as a decoy for HBV-specific CD8+ T cells, sparing HBV-infected hepatocytes from recognition. Clearly, these data need to be confirmed for other HBV epitopes restricted by different HLA-class I molecules and in larger population of CHB patients. Nevertheless, if HBV-DNA integration represents the major and constant source of newly synthetized HBsAg, particularly in anti-HBe+ CHB patients (26), the possibility that envelope-specific CD8+ T cells in anti-HBe+ patients would preferentially target hepatocytes with HBV-DNA integration and not with productive HBV infection appears possible.

335 On the other hand, the efficient and consistent presentation of viral epitopes derived
336 from HBV-DNA integration might open a therapeutic opportunity for the treatment of
337 HBV-related hepatocellular carcinoma. We have already shown that T cells engineered
338 with HBV-specific T cell receptors can target HBV antigens in HCC cells with HBV-DNA
339 integration (38). Understanding the efficiency of HBV epitope presentation in HBV-
340 infected primary hepatocytes or tumor cells carrying HBV-DNA integration will allow the
341 generation of engineered CD8+ T cells with T cell receptors specific for epitopes mainly
342 produced by HCC cells and not by HBV-infected hepatocytes.
343 There are several limitations in this study. First we defined the differential distribution of
344 two HBV epitopes in the biopsies of only two CHB patients. Our TCR-like antibodies
345 detect HBV epitopes originated from HBV genotype D patients and as such the pool of
346 HLA-A*02:01+ CHB patients showing a positive staining with both TCR-like antibodies
347 was reduced to only 3 CHB patients. Furthermore, only in two patients the consecutive
348 sections stained with the two different HBV epitopes have an identical morphology that
349 allow us to compare the topological localization of two different HBV epitopes. In
350 addition, the differential distribution of core and envelope epitopes was detected in CHB
351 patients that were anti-HBe+. Since the quantity of HBsAg produced from HBV-DNA
352 integration has been shown to be predominant in this CHB patient population(26),
353 future studies will be necessary to define whether the mosaic distribution of different
354 HBV epitopes can be generalized to other CHB patients populations.

355 In addition, the TCR-like antibodies used here limited our analysis to the HLA-A*02:01-
356 restricted HBc18-27 and HBs183-91 epitopes . Although these epitopes are important in
357 HLA-A*02:01^{+}subjects (31), they might not be representative of other nucleocapsid or
358 envelope epitopes restricted by different HLA-class I molecules.

For example, a core-derived HBV epitope restricted by HLA-A68w and HLA-A31 requires the activation of the immunoproteasome (20). This clearly differs from our results indicating that HBc18-27 epitope remains unchanged upon treatment with IFN-γ. Similarly, we doubt that all envelope derived epitopes restricted by different HLA-class I will follow the same pattern of presentation as the HBs183-191 epitope reported here. For example, the clear dominance of the HLA-Cw0801-epitope HBs178-185 detected in Asian populations (39) might suggest that its generation is mediated by constitutive proteasome activity like the immunodominant HLA-A*02:01/ HBc18-27.

Nevertheless, the differences in the presentation efficiency of the two HBV epitopes described here suggest that during natural infection, HBV-specific CD8+ T cells of different specificities might target selected HBV antigen-expressing hepatocytes with different efficacy within an infected liver. These findings called for a deeper understanding of the HBV epitope hierarchy of presentation across different HLA-class I backgrounds in order to design immunological strategies to control chronic HBV infection or HBV-related HCC in patients.

Material and Methods

Cell Lines

Table 2 lists the biological features of cell lines used in the experimental settings.

Briefly, human liver cancer line HepG2 (ATCC), HepG2-hNTCP-A3 **(**HepG2 cells transduced with human NTCP) (14) and HepG2.2.15 (HepG2 cells transduced with full HBV genome) (10), were maintained in DMEM supplemented with 10% heat-inactivated fetal bovine serum (FBS), 100 U/ml of penicillin, 100 µg/ml of streptomycin and Glutamax (Invitrogen, Carlsbad, CA). HepG2-hNTCP-A3 and HepG2.2.15 were selected

using 5 µg/ml of puromycin (BD Biosciences, San Jose, CA) and 200 µg/ml geneticin (G418 disulfate salt) (Sigma-Aldrich, St. Louis, MO), respectively.

HepG2-Env (35), PLC/PRF5/A2+ (PLC/PRF5 (36) transduced with HLA-A*02:01) and EBV core (EBV-transformed B lymphoblastoid cell line transduced with full HBV core) (8) were maintained in RPMI 1640 supplemented with 10% heat-inactivated FBS, 20 mM HEPES, 0.5 mM sodium pyruvate, 100 U/ml penicillin, 100 µg/ml streptomycin, MEM amino acids, Glutamax and MEM nonessential amino acids (Invitrogen, Carlsbad,CA). HepG2-Env and PLC/PRF5/A2+ were selected using 5µg/ml of puromycin. EBV core cells were selected using 250ug/ml hygromycin (Sigma-Aldrich).

HepAD38 cells, used for virus particle production, were cultured in DMEM with 10% tetracycline-free FBS, 100 U/ml penicillin/streptomycin, 2mM L-glutamine and 0.4 ug/ml doxycycline(41).

Primary human hepatocyte (PHH) culture

Fresh HLA-A*0201^{+} PHH were obtained from humanized FRG mouse model (Invitrocue, Singapore). PHH were maintained in a distinct density according to the manufacturer protocol in Hepacur medium (Invitrocue, Singapore) containing 2% DMSO in 37 ºC with 5% CO2 all through the experiment.

HBV virus production

Briefly, to induce virus particle production in HepAD38 (HBV genotype D), doxycycline was removed from the medium, fresh medium replaced and after 20 days, HBV DNA titres were measured from the supernatant by qPCR, according to manufacturer's instructions, using Qiagen HBV Artus PCR kit (Qiagen). Virus particles were subsequently concentrated using a commercial polyethylene glycol (PEG) precipitation kit (Abcam) according to manufacturer's protocol, which resulted in approximately 50-100 fold concentration of virus stock.

HBV infection

HepG2-hNTCP-A3 cells at 70% confluency and PHH at day 1 post seeding were inoculated with approximately 50-100 fold concentrated supernatant of HepAD38 as HBV inoculum (genotype D) at multiplicities of GEV 3000/cell in 4% PEG (Sigma–Aldrich) medium for 24 hours at 37 ºC with 5% CO2. Inoculum was removed subsequently and cells were washed with 1XPBS, three times. Infection efficiency was quantified at 12 hours, 18hours, days 1, 3, 7 for both HepG2-hNTCP-A3 and PHH after removal of inoculum, referred to as time post-infection.

Co-culture experiment of HBV specific CD8+ T cells with targets

Two HLA-A*02:01 CD8+ T cell lines specific to HBV epitopes core18-27 (HBc18-27), S183-91 (HBs183-91) were generated from HLA-A02:01^{+} patients with acute hepatitis infection and maintained in vitro as described previously (40).

The activation of HBV-specific CD8+ T cells was tested by measuring degranulation (CD107a) and cytokine production (IFN-γ and TNF-α) through surface and intracellular staining, respectively. Briefly, CD8+ T cells were incubated with different cell lines for 5 hours in the presence of Brefeldin A (BFA) (10 µg/ml) and CD107a-FITC (BD Biosciences) at E:T ratio of 1:2 at 37 ºC with 5% CO2. After washing, cells were subjected to surface and intracellular staining.

Both CD8+ T cell clones were activated by HepG2.2.15 (HepG2 cells with full HBV genome integration) (10), demonstrating their ability to recognize HBV epitopes produced from endogenously synthetized HBV antigens (data not shown). Analysis of functional affinity of the CD8+ T cell clones showed that HBc18-27 and HBs183-91 specific CD8+ T cells can recognize target cells (HLA-A*02:01+ EBV-immortalized B cells) pulsed with peptide concentration as low as 1-10pM.

Surface and Intracellular staining

HBV specific CD8+ T cell activation:

Upon 5 hours incubation with CD8+ T cell clones in the presence of CD107a and BFA (as described earlier), cells were stained with anti-CD8 V500 (Biolegend) for 30 min at 4°C followed by standard intracellular staining protocol. Briefly, cells were fixed and permeabilized for 30 min at 4°C (CytoFix/Cytoperm, BD Biosciences), followed by staining with mouse anti human IFN-γ PE-CY7 (Biolegend) and mouse anti human TNF-α PE (BD Biosceinces) for 30 min at 4°C . Finally, cells were fixed in 1% PFA in 1X PBS and cell acquisition was done using BD LSR-II flow cytometer and data were analyzed in FACS Diva software.

HBV infection efficiency:

HBV-infected or un-infected cells at different times post-infection were fixed and permeabilized for 30 min at 4°C (CytoFix/Cytoperm, BD Biosciences). Cells were then stained with primary antibodies, rabbit HBcAg (Thermofisher scientific) and mouse HBsAg (RayBiotech) for 30 min at 4°C. This was followed by 30 min staining using secondary antibodies goat anti-rabbit –CF55 (Sigma-Aldrich) and goat anti-mouse APC (Invitrogen) at 4°C. Cells were then fixed at 1% PFA in 1X PBS and acquisition was done using BD LSR-II flow cytometer and data were analyzed in FACS Diva software.

HBV-epitope/HLA-A*02:01 complex quantification

Two antibodies specific to HBc18-27 and HBs183-91/ HLA-A*02:01 complexes were used for staining PHH, hepatocyte-like cell lines and liver biopsies. Their production and specificity was described previously (17). Since they recognize the complexes HBV-peptide/HLA-A*02:01 molecules like a T cell receptor of T cells, we defined them as TCR-like antibodies.

In-vitro HBV infection system:

457 Flow cytometry analysis:

458 Infected or un-infected cells were stained with Aqua LIVE/DEAD fixable dead cell stain
459 kit (Invitrogen) for 10 min at room temperature (RT) followed by staining with TCR-like
460 antibodies for 1 hour. Cells were then stained with goat anti-mouse APC secondary
461 antibody (Invitrogen). Cells were then subjected to an APC FASER amplification kit
462 (Miltenyi Biotech). This was followed with intracellular staining for HBcAg (as described
463 earlier). APC mean fluorescence intensity (MFI) in cells positive for HBcAg was
464 analyzed using BD LSR-II flow cytometer. Data analysis was done using FACS Kaluza
465 software (Beckman Coulter).

466 Image stream analysis:

467 Infected or un-infected cells were stained with TCR like antibodies for 1 hour followed by
468 staining with goat anti-mouse APC secondary antibody for 30 min. APC signal was
469 amplified as described earlier. MFI of APC was then analyzed using Image Stream
470 analyser. Images were analyzed using the IDEAS 4.0 software.

471 *Liver Biopsy tissue staining:*

472 TCR-like mAb staining

473 Briefly, human liver biopsy samples from 8 HLA-A*02:01 patients as described in table
474 1, were kept frozen in OCT (VWR Chemicals) before staining. Tissues were then
475 sectioned (5µm) and fixed in acetone for 30 min followed by air-drying for 10 min.
476 Samples were then washed with 1X PBS followed by two-step blocking with Dual
477 Endogenous enzyme block (DAKO, Agilent Technologies) and 2% BSA in 1XPBS at RT
478 for 10 and 30 min, respectively. Tissues were incubated with above mentioned TCR-like
479 antibodies overnight at 4ºC. This was followed by anti-mouse secondary antibody
480 staining using EnVision+ System-HRP labelled polymer (DAKO, Agilent Technologies),

for 30 min at RT. Tissues were then subjected to a Tyramide staining -Alexa Fluor 647 (Thermo Fisher Scientific) amplification kit, followed by co-staining with a mouse anti-human cytokeratin18-FITC (Miltenyi Biotech) and nuclei staining with DAPI. Whole-tissue scanning and fluorescence microscopy was performed on an automated scanning workstation (TissueFAXS; Tissue Gnostics).

Viral antigen staining in liver biopsies

Tissue biopsy kept in OCT (as mentioned previously) were sectioned (5uM) and washed with 1XPBS. Slides were then blocked and permeabilized using 3% mouse sera 1% BSA, 0.25% Saponin in 1X PBS. This was followed with staining of tissue sections with primary antibody goat anti-HBsAg (Abcam) overnight at 4°C. Tissue sections were then subjected to staining with secondary antibody, rabbit anti-goat APC coupled with Cytokeratin 18-FITC conjugated antibody (Miltenyi Biotech). Cells were then stained with DAPI for nuclei staining. Images were captured using whole-tissue scanning and fluorescence microscopy on an automated scanning workstation (TissueFAXS; Tissue Gnostics)

Immunofluorescence staining

HBV-infected HepG2-hNTCP-A3 cells were seeded on cover slips at $2x10^5$ cells density. At indicated days post-infection, cells were washed with 1XPBS and fixed with 4% PFA for 10 min. Upon permeabilization, cells were stained using primary antibodies rabbit anti-HBcAg (Abcam) and mouse anti-HBsAg (RayBiotech) followed by secondary antibodies goat anti-rabbit CF633 (Sigma-Aldrich) and goat anti mouse AF-488 (Invitrogen). Cell nuclei were then stained with DAPI and images were acquired using Carl Zeiss confocal laser scanning upright microscope.

NanoString gene expression analysis

Targets with HBV-DNA integration as well as HBV-infected or un-infected cells were lysed in RLT lysis buffer (QIAGEN, supplemented with 2-mercaptoethanol at 1:100) according to Nanostring Technologies guidelines. Lysate of at least 20000 cells were analyzed using the customized nCounter GX human Immunology Kit coupled with probes specific to HBV viral RNA. Probe set specific to HBV viral RNA were designed according to Nanostring nCounter Technology guidelines (Nanostring Technologies, Seattle, WA) to specific regions on the HBV genome as shown in Fig 2b.

The background detection and normalization of data was done using the n-Solver analysis software 3.0 based on the geometric mean of the supplied positive and negative controls and the housekeeping gene panel**.**

Statistics

Statistical significance was evaluated with 2-tailed *t* test and, where appropriate, one way or 2-way ANOVA with Tukey's or Dunnett's multiple comparisons test using the data analysis software Prism 6. Only *P* values and adjusted *P* values (ANOVA) of less than 0.05 were considered significant and displayed in the figures.

Ethic Statement

Written informed consent was obtained prior to collection of liver samples. The study was approved by Barts and the London NHS Trust local ethics review board and NRES committee London – REC reference 10/H0715/39.

Acknowledgements

We would like to thank Prof. Christoph Seeger (FOX Chase Cancer Center, Philadelphia, Pennsylvania, United States of America) for the HepAD38 cell line used in virus particle production. We also thank Singhealth Duke-NUS advanced Bioimaging

core facility for their assistance. This work was supported by a Singapore Translational Research (STaR) Investigator Award (NMRC/STaR/013/2012) to A.B.

References

1. **Germain RN**. 1994. MHC-dependent antigen processing and peptide presentation: providing ligands for T lymphocyte activation. Cell **76**:287–299.

2. **Yewdell JW**. 2006. Confronting Complexity: Real-World Immunodominance in Antiviral CD8+ T Cell Responses. Immunity **25**:533–543.

3. **Hewitt EW**. 2003. The MHC class I antigen presentation pathway: strategies for viral immune evasion. Immunology **110**:163–169.

4. **Thimme R**, **Wieland S**, **Steiger C**, **Ghrayeb J**, **Reimann KA**, **Purcell RH**, **Chisari FV**. 2003. CD8(+) T cells mediate viral clearance and disease pathogenesis during acute hepatitis B virus infection. Journal of Virology **77**:68–76.

5. **Kah J**, **Koh S**, **Volz T**, **Ceccarello E**, **Allweiss L**, **Lütgehetmann M**, **Bertoletti A**, **Dandri M**. 2017. Lymphocytes transiently expressing virus-specific T cell receptors reduce hepatitis B virus infection. J Clin Invest **127**:3177–3188.

6. **Winer BY**, **Huang TS**, **Pludwinski E**, **Heller B**, **Wojcik F**, **Lipkowitz GE**, **Parekh A**, **Cho C**, **Shrirao A**, **Muir TW**, **Novik E**, **Ploss A**. 2017. Long-term hepatitis B infection in a scalable hepatic co-culture system. Nat Comm **8**:125.

7. **Bertoletti A**, **Ferrari C**, **Fiaccadori F**, **Penna A**, **Margolskee R**, **Schlicht HJ**, **Fowler P**, **Guilhot S**, **Chisari FV**. 1991. HLA class I-restricted human cytotoxic T cells recognize endogenously synthesized hepatitis B virus nucleocapsid antigen. Proc Natl Acad Sci USA **88**:10445–10449.

8. **Guilhot S**, **Fowler P**, **Portillo G**, **Margolskee RF**, **Ferrari C**, **Bertoletti A**, **Chisari FV**. 1992. Hepatitis B virus (HBV)-specific cytotoxic T-cell response in humans: production of target cells by stable expression of HBV-encoded proteins in immortalized human B-cell lines. J Virol **66**:2670–2678.

9. **Huang LR**, **Gäbel YA**, **Graf S**, **Arzberger S**, **Kurts C**, **Heikenwalder M**, **Knolle PA**, **Protzer U**. 2012. Transfer of HBV genomes using low doses of adenovirus vectors leads to persistent infection in immune competent mice. Gastroenterology **142**:1447–50.e3.

10. **Sun D**, **Nassal M**. 2006. Stable HepG2- and Huh7-based human hepatoma cell lines for efficient regulated expression of infectious hepatitis B virus. J Hepatol **45**:636–645.

11. **Moriyama T**, **Guilhot S**, **Klopchin K**, **Moss B**, **Pinkert CA**, **Palmiter RD**, **Brinster RL**, **Kanagawa O**, **Chisari FV**. 1990. Immunobiology and pathogenesis of hepatocellular injury in hepatitis B virus transgenic mice. Science **248**:361–364.

12. **Guidotti LG**, **Ishikawa T**, **Hobbs MV**, **Matzke B**, **Schreiber R**, **Chisari FV**. 1996. Intracellular inactivation of the hepatitis B virus by cytotoxic T lymphocytes. Immunity

4:25–36.

13. **Yan H**, **Zhong G**, **Xu G**, **He W**, **Jing Z**, **Gao Z**, **Huang Y**, **Qi Y**, **Peng B**, **Wang H**, **Fu L**, **Song M**, **Chen P**, **Gao W**, **Ren B**, **Sun Y**, **Cai T**, **Feng X**, **Sui J**, **Li W**. 2012. Sodium taurocholate cotransporting polypeptide is a functional receptor for human hepatitis B and D virus. eLife **1**:e00049–e00049.

14. **Ni Y**, **Lempp FA**, **Mehrle S**, **Nkongolo S**, **Kaufman C**, **Fälth M**, **Stindt J**, **Königer C**, **Nassal M**, **Kubitz R**, **Sültmann H**, **Urban S**. 2014. Hepatitis B and D viruses exploit sodium taurocholate co-transporting polypeptide for species-specific entry into hepatocytes. Gastroenterology **146**:1070–1083.

15. **Hoh A**, **Heeg M**, **Ni Y**, **Schuch A**, **Binder B**, **Hennecke N**, **Blum HE**, **Nassal M**, **Protzer U**, **Hofmann M**, **Urban S**, **Thimme R**. 2015. Hepatitis B Virus-Infected HepG2hNTCP Cells Serve as a Novel Immunological Tool To Analyze the Antiviral Efficacy of CD8+ T Cells In Vitro. J Virol **89**:7433–7438.

16. **Makarova-Rusher OV**, **Medina-Echeverz J**, **Duffy AG**, **Greten TF**. 2015. The yin and yang of evasion and immune activation in HCC. J Hepatol **62**:1420–1429.

17. **Sastry KSR**, **Too CT**, **Kaur K**, **Gehring AJ**, **Low L**, **Javiad A**, **Pollicino T**, **Li L**, **Kennedy PTF**, **Lopatin U**, **Macary PA**, **Bertoletti A**. 2011. Targeting hepatitis B virus-infected cells with a T-cell receptor-like antibody. J Virol **85**:1935–1942.

18. **Ji C**, **Sastry KSR**, **Tiefenthaler G**, **Cano J**, **Tang T**, **Ho ZZ**, **Teoh D**, **Bohini S**, **Chen A**, **Sankuratri S**, **Macary PA**, **Kennedy P**, **Ma H**, **Ries S**, **Klumpp K**, **Kopetzki E**, **Bertoletti A**. 2012. Targeted delivery of interferon-α to hepatitis B virus-infected cells using T-cell receptor-like antibodies. Hepatology **56**:2027–2038.

19. **Bertoletti A**, **Ferrari C**. 2016. Adaptive immunity in HBV infection. J Hepatol **64**:S71–83.

20. **Sijts AJ**, **Ruppert T**, **Rehermann B**, **Schmidt M**, **Koszinowski U**, **Kloetzel PM**. 2000. Efficient generation of a hepatitis B virus cytotoxic T lymphocyte epitope requires the structural features of immunoproteasomes. J Exp Med **191**:503–514.

21. **Chu CM**, **Liaw YF**. 1992. Immunohistological study of intrahepatic expression of hepatitis B core and E antigens in chronic type B hepatitis. J Clin Pathol **45**:791–795.

22. **Chu CM**, **Yeh CT**, **Sheen IS**, **Liaw YF**. 1995. Subcellular localization of hepatitis B core antigen in relation to hepatocyte regeneration in chronic hepatitis B. Gastroenterology **109**:1926–1932.

23. **Zhang X**, **Lu W**, **Zheng Y**, **Wang W**, **Bai L**, **Chen L**, **Feng Y**, **Zhang Z**, **Yuan Z**. 2016. In situ analysis of intrahepatic virological events in chronic hepatitis B virus infection. J Clin Invest **126**:1079–1092.

24. **Safaie P**, **Poongkunran M**, **Kuang P-P**, **Javaid A**, **Jacobs C**, **Pohlmann R**, **Nasser I**, **Lau DTY**. 2016. Intrahepatic distribution of hepatitis B virus antigens in patients with and without hepatocellular carcinoma. World J Gastroenterol **22**:3404–3411.

25. **Larsson SB**, **Malmström S**, **Hannoun C**, **Norkrans G**, **Lindh M**. 2015. Mechanisms downstream of reverse transcription reduce serum levels of HBV DNA but not of HBsAg in chronic hepatitis B virus infection. Virology Journal **12**:2053–8.

26. **Wooddell CI**, **Yuen M-F**, **Chan HL-Y**, **Gish RG**, **Locarnini SA**, **Chavez D**, **Ferrari C**,

Given BD, **Hamilton J**, **Kanner SB**, **Lai C-L**, **Lau JYN**, **Schluep T**, **Xu Z**, **Lanford RE**, **Lewis DL**. 2017. RNAi-based treatment of chronically infected patients and chimpanzees reveals that integrated hepatitis B virus DNA is a source of HBsAg. Sci Trans Med **9**:eaan0241.

27. **Rehermann B**, **Fowler P**, **Sidney J**, **Person J**, **Redeker A**, **Brown M**, **Moss B**, **Sette A**, **Chisari FV**. 1995. The cytotoxic T lymphocyte response to multiple hepatitis B virus polymerase epitopes during and after acute viral hepatitis. J Exp Med **181**:1047–1058.

28. **Maini MK**, **Boni C**, **Lee CK**, **Larrubia JR**, **Reignat S**, **Ogg GS**, **King AS**, **Herberg J**, **Gilson R**, **Alisa A**, **Williams R**, **Vergani D**, **Naoumov NV**, **Ferrari C**, **Bertoletti A**. 2000. The role of virus-specific CD8(+) cells in liver damage and viral control during persistent hepatitis B virus infection. J Exp Med **191**:1269–1280.

29. **Fisicaro P**, **Barili V**, **Montanini B**, **Acerbi G**, **Ferracin M**, **Guerrieri F**, **Salerno D**, **Boni C**, **Massari M**, **Cavallo MC**, **Grossi G**, **Giuberti T**, **Lampertico P**, **Missale G**, **Levrero M**, **Ottonello S**, **Ferrari C**. 2017. Targeting mitochondrial dysfunction can restore antiviral activity of exhausted HBV-specific CD8 T cells in chronic hepatitis B. Nat Med **23**:327–336.

30. **Pallett LJ**, **Davies J**, **Colbeck EJ**, **Robertson F**, **Hansi N**, **Easom NJW**, **Burton AR**, **Stegmann KA**, **Schurich A**, **Swadling L**, **Gill US**, **Male V**, **Luong T**, **Gander A**, **Davidson BR**, **Kennedy PTF**, **Maini MK**. 2017. IL-2(high) tissue-resident T cells in the human liver: Sentinels for hepatotropic infection. J Exp Med **214**:1567–1580.

31. **Tan AT**, **Loggi E**, **Boni C**, **Chia A**, **Gehring AJ**, **Sastry KSR**, **Goh V**, **Fisicaro P**, **Andreone P**, **Brander C**, **Lim SG**, **Ferrari C**, **Bihl F**, **Bertoletti A**. 2008. Host ethnicity and virus genotype shape the hepatitis B virus-specific T-cell repertoire. J Virol **82**:10986–10997.

32. **Mutz P**, **Metz P**, **Lempp FA**, **Bender S**, **Qu B**, **Schöneweis K**, **Seitz S**, **Tu T**, **Restuccia A**, **Frankish J**, **Dächert C**, **Schusser B**, **Koschny R**, **Polychronidis G**, **Schemmer P**, **Hoffmann K**, **Baumert TF**, **Binder M**, **Urban S**, **Bartenschlager R**. 2018. HBV Bypasses the Innate Immune Response and Does Not Protect HCV From Antiviral Activity of Interferon. Gastroenterology **154**:1791–1804.e22.

33. **Kloetzel PM**. 2001. Antigen processing by the proteasome. Nat Rev Mol Cell Biol **2**:179–187.

34. **Gehring AJ**, **Haniffa M**, **Kennedy PT**, **Ho ZZ**, **Boni C**, **Shin A**, **Banu N**, **Chia A**, **Lim SG**, **Ferrari C**, **Ginhoux F**, **Bertoletti A**. 2013. Mobilizing monocytes to cross-present circulating viral antigen in chronic infection. J Clin Invest **123**:3766–3776.

35. **Pavesi A**, **Tan AT**, **Koh S**, **Chia A**, **Colombo M**, **Antonecchia E**, **Miccolis C**, **Ceccarello E**, **Adriani G**, **Raimondi MT**, **Kamm RD**, **Bertoletti A**. 2017. A 3D microfluidic model for preclinical evaluation of TCR-engineered T cells against solid tumors. JCI Insight **2**.

36. **Aden DP**, **Fogel A**, **Plotkin S**, **Damjanov I**, **Knowles BB**. 1979. Controlled synthesis of HBsAg in a differentiated human liver carcinoma-derived cell line. Nature **282**:615–616.

37. **Nayersina R**, **Fowler P**, **Guilhot S**, **Missale G**, **Cerny A**, **Schlicht HJ**, **Vitiello A**, **Chesnut R**, **Person JL**, **Redeker AG**, **Chisari FV**. 1993. HLA A2 restricted cytotoxic T lymphocyte responses to multiple hepatitis B surface antigen epitopes during hepatitis B virus infection. J Immunol **150**:4659–4671.

38. **Qasim W**, **Brunetto M**, **Gehring AJ**, **Xue S-A**, **Schurich A**, **Khakpoor A**, **Zhan H**, **Ciccorossi P**, **Gilmour K**, **Cavallone D**, **Moriconi F**, **Farzhenah F**, **Mazzoni A**, **Chan L**, **Morris E**, **Thrasher A**, **Maini MK**, **Bonino F**, **Stauss H**, **Bertoletti A**. 2015. Immunotherapy of HCC metastases with autologous T cell receptor redirected T cells, targeting HBsAg in a liver transplant patient. J Hepatol **62**:486–491.

39. **Tan AT**, **Sodsai P**, **Chia A**, **Moreau E**, **Chng MHY**, **Tham CYL**, **Ho ZZ**, **Banu N**, **Hirankarn N**, **Bertoletti A**. 2014. Immunoprevalence and immunodominance of HLA-Cw*0801-restricted T cell response targeting the hepatitis B virus envelope transmembrane region. J Virol **88**:1332–1341.

40. **Gehring AJ**, **Sun D**, **Kennedy PTF**, **Nolte-'t Hoen E**, **Lim SG**, **Wasser S**, **Selden C**, **Maini MK**, **Davis DM**, **Nassal M**, **Bertoletti A**. 2007. The Level of Viral Antigen Presented by Hepatocytes Influences CD8 T-Cell Function. J Virol **81**:2940–2949.

41. **Ladner SK**, **Otto MJ**, **Barker CS**, **Zaifert K**, **Wang GH**, **Guo JT**, **Seeger C**, **King RW**. 1997. Inducible expression of human hepatitis B virus (HBV) in stably transfected hepatoblastoma cells: a novel system for screening potential inhibitors of HBV replication. Antimic Agents Chemiot 41:1715-1720.

Figure legends

Figure 1: Spatial distribution of HLA/HBV epitope complexes in HBV chronically infected livers Comparative analysis of CHB patients' liver biopsies demonstrated a non-uniform distribution of HBV epitope presentation in liver parenchyma.

(a-d) Consecutive sections of two CHB patient liver biopsies (Patient number 1 and 2 in table 1), stained with isotype control antibody (anti mouse IgG-APC), TCR-like antibody specific for HLA-A*02:01/HBs183-91 (labelled as A2-HBs183) and for HLA-A*02:01/HBc18-27 (labelled as A2-HBc18) complexes and with anti-HBs antibody (Insert b and d). Regions positive for antibodies staining (TCR-like and anti-HBs antibodies) are in red, hepatocytes are stained with cytokeratin 18 in green, and nucleus of cells is stained with DAPI in blue. The images are captured using TissueFAXS immunofluorescent microscopy.

680 A schematic representation of the distribution of the two HLA-A*02:01/HBV epitope
681 complexes in hepatic parenchyma of patient 1 is shown. Region A marks fibrotic portal
682 region. Region B indicates parts only positive for A2-HBc18 complexes while region C is
683 positive for A2-HBs183 complexes. Region D and E mark regions respectively negative
684 or positive for both HLA/HBV epitopes complexes. Region E marks the region positive
685 for both A2-HBc18 and A2-HBs183 complexes.

686 **(e)** Representative liver biopsy images of a HLA-A*02:01 positive patient infected with
687 HBV genotype C (patient number4 in table 1), stained with TCR-like antibodies.
688 Inserted Tables summarize the clinical and virological features of each patient.

689

690 **Figure 2: Establishment of *in vitro* HBV infection in PHH and HepG2-hNTCP-A3**
691 **cells**

692 **(a)** Schematic representation of the experimental procedure utilized to infect HepG2-
693 hNTCP-A3 and PHH. Cells were inoculated at multiplicities of GEV 3000/cell for 24
694 hours. Cells were utilized for virological and immunological assays at the indicated times
695 after removal of the inoculum (time 0) referred to as time post-infection.

696 **(b)** Nanostring probes specific to HBV 3.5kb mRNA (pgRNA) (3.5Kb mRNA probe), HBV
697 large S (S probe) and HBV core (Core probe) mRNA are designed. Map represents the
698 regions on the HBV genome which is covered by each probe.

699 **(c and d)** Probes specificity were tested in cells with over-expression of individual HBV
700 protein or full HBV-DNA integration: HepG2-Env and HepG2.2.15 (See Table 2). Bars
701 show normalized counts for the indicated mRNA obtained by nanostring technology in
702 each cell line. The highest count in each cell line belongs to the probe more specific to
703 the region of the HBV protein which the different cell lines are overexpressing. **(c)**

HepG2-Env cell lines shows higher counts for the probe specific to a region of large S. **(d)** Highest counts of the probe specific to HBV 3.5 kb mRNA (pgRNA) is observed in HepG2.2.15, which has active HBV replication.

(e) HBV 3.5 kb mRNA expression in PHH (left) and HepG2-hNTCP-A3 (right) infected cells at indicated length of infection. Bars represent the normalized counts of HBV 3.5 kb mRNA (pgRNA) obtained using nanostring technology.The indicated p values represent the significant increase of viral replication over the time of infection (Mean of 3 replicates) .

(f) Frequency of HBV-infected (solid lines) or un-infected (dotted lines) cells in PHH (right) and HepG2-hNTCP-A3 (left). Cells expressing HBcAg (blue) or HBsAg (green) at 12 hours, 18 hours and day 1, 3 and 7 post-infection are measured with anti-HBs and anti-HBc specific antibodies by flow cytometry analysis. A gradual increase in frequency of HBcAg/HBsAg positive cells is observed in both PHH and HepG2-hNTCP-A3 over infection time.

(g) HLA-class I surface expression in HBV-infected PHH (top) and HepG2-hNTCP-A3 (bottom) cells measured using flow cytometry. The surface expression of HLA-class I is compared to un-infected target cells over time (day 1-7).

Figure 3: HLA/HBV epitope complexes presentation on HBV-infected PHH and HepG2-hNTCP-A3

(a) Schematic representation of HBV infected PHH or HepG2-hNTCP-A3 utilized for immunological assays.

(b) Quantity of HLA-A*02:01/HBV epitope complexes on the HBcAg negative and positive on HBV infected cells is measured using two TCR-like mAb, A2-HBc18 and A2-HBs183, by flow cytometry analysis. On left, shown is the gating strategy. Histogram

displays a representative MFI of TCR-like antibodies measured on gated cells positive or negative for HBcAg staining (using anti-HBc antibody) (L/D stands for Live/dead). The representative dot plot on the right shows the staining profile of double positive population for HBcAg (X axis) and TCR-like mAb (Y axis). On right, bars show MFI values of A2-HBc18 (blue) and A2-HBs183 (green) on HBcAg+ cells in comparison with the HBcAg- population in both PHH (top) and HepG2-hNTCP-A3 (bottom) infected cells. Dots represents individual experiments. At least two replicates for indicated time points were performed.

(c) The surface distribution of A2-HBc18 is shown on HepG2-hNTCP-A3 cells infected for 7 days post-infection in comparison with HepG2 cells pulsed with 1ug/ml of HBc18-27 peptide, using Image Stream analyser. Representative images of cells show clustered distribution of complexes on infected targets as oppose to peptide pulsed ones. Un-infected cells show negative background staining. BF = bright field, APC= fluorescent field

(d) Ability of HBc18-27 (blue bars) and HBs183-91 (green bars) specific CD8+ T cells to recognize PHH and HepG2-hNTCP-A3 infected with HBV for the indicated times. Bars show the frequency of CD107a-expressing CD8+ T cells (top panels), activated IFN-γ (second row panels) or TNF-α (bottom panels) positive CD8+ T cells among total CD8+ T cells after being co-cultured for 5 hours with E:T ratio of 1:2. All data shown as the mean $\pm$ SD of at least 3 independent experiments.

Figure 4: The effect of IFN-γ on HBV-epitopes presentation

(a) Schematic of experimental procedure of IFN-γ pulsing (100IU/ml - 48 hours) of HBV infected HepG2-hNTP-A3 and PHH .

751 **(b)** Direct quantification of HLA-class I/HBV epitope complexes with Abs specific for A2-
752 HBc18(blue) and A2-HBs183(green) complexes in HBV-infected PHH (left panels) or
753 HepG2-hNTCP-A3 (right panels) with or without IFN-γ. Bars show MFI of HBcAg+
754 population in untreated infected cells (dark shades) compared with IFN-γ treated ones
755 (shown in brighter shades).

756 **(c)**Representative histogram plots of day 3 post-infection showing MFI of A2-HBc18
757 (blue) and A2-HBs183 (green) complexes on cell surface of HBcAg- (Top panels) and
758 HBcAg+ cells (bottom panels) in infected PHH (left) or HepG2-hNTCP-A3 cells (right).
759 In each Histogram the MFI of TCR-like mAb is shown in the presence (dotted lines) or
760 absence (solid lines) of IFN-γ treatment.

761 **(d)** Ability of CD8+ T cells specific for HBc18-27 (blue bars) and HBs183-91 (green bars)
762 to recognize infected PHH or HepG2-hNTCP-A3 for the indicated duration, with (brighter
763 shades) or without (dark shade) IFN-γ treatment (100 IU/ml, for 48 hrs). Bars represent
764 frequency of CD8+ T cells expressing CD107a among total CD8+ T cells co-cultured
765 with PHH (top) and HepG2-hNTCP-A3 (bottom) for 5 hours at E:T ratio of 1:2 . All data
766 shown as the mean ± SD of at least 3 independent experiments.

767 **Figure 5: HBV-epitope presentation requires NTCP-mediated infection and viral**
768 **protein synthesis**

769 **(a)** Schematic representation of infection of HepG2-hNTCP-A3 and PHH in the presence
770 or absence of 800nM Myrcludex B (MyrB)

771 **(b)** Frequency of HBV-specific CD8+ T cells expressing CD107a among total CD8+ T
772 cells after 5 hours of co-culture (E:T ratio = 1:2) with infected PHH (left panels) or
773 HepG2-hNTCP-A3 (right panels) at day 1 post-infection. Targets are infected in the

774 presence or absence of MyrB. In addition cells were either treated with IFN-γ or left
775 untreated as described in Fig 4.

776 **(c)** Ability of CD8+ T cells specific for HBc18-27 (blue bars) or HBs183-91 (green bars)
777 to recognize HepG2-hNTCP-A3 infected with HBV or UV inactivated HBV, in the
778 presence or absence of IFN-γ. Bars show CD8+ T cells positive for CD107a among total
779 CD8+ T cells after 5 hours of co-culture with target cells at day 1 post-infection, E:T ratio
780 = 1:2. Data shown as mean ± SD of two independent experiments.

781 **(d)** Expression of HBcAg (blue bars) and HBsAg (green bars) in the presence or
782 absence of MyrB treatment in both PHH (top) and HepG2-hNTCP-A3 (bottom) infected
783 targets at day 1 p.i is shown. Targets are either treated with IFN-γ (brighter shades) or
784 un-treated (darker shades).

785 **(e)** Frequency of CD107a positive CD8+ T cells specific for HBc18-27 (blue bars) and
786 HBs183-91 (green bars), co-cultured with HBV infected (darker shades) or un-infected
787 (brighter shades) HepG2-hNTCP-A3 treated or un -treated with 10µM Lamivudine .
788 Data related to day3 post infection.

789 **Figure 6: Superior HBV CD8+ T cell epitope presentation on targets producing**
790 **HBV antigens from HBV-DNA integration**

791 **(a)** Direct quantification of A2-HBs183 complexes on the surface of hepatoma cells with
792 HBV-DNA integration (HepG2.2.15, HepG2-Env, PLC/PRF5-A2+) in comparison with
793 infected HepG2-hNTCP-A3 at day 7 post-infection treated or untreated with IFN-γ. Cells
794 were stained with A2-HBs183 antibody as indicated previously. Bars show MFI of
795 indicated antibody measured by Image Stream analyser.

(b) Bars show MFI of A2-HBc18 complexes on the surface of cells with full HBV genome integration, HepG2.2.15 in comparison with infected HepG2-hNTCP-A3 cells at day 7 post-infection in the presence or absence of IFN-γ. MFI is measured using Image Stream analyser.

(c) Ability of HBs183-91 specific CD8+ T cells to recognize target cells with HBV-DNA integration (HepG2.2.15, HepG2-Env, PLC/PRF5-A2+) and HBV-infected HepG2-hNTCP-A3 (day 7 post-infection with or without IFN-γ treatment). Bars represent activation of CD8+ T cells measured through CD107a expression.

(d) Expression of HBV large S mRNA is quantified on target cells with HBV-DNA integration (HepG2.2.15, HepG2-Env and PLC/PRF5-A2+). Bars represent the numeric normalized count of mRNA measured by nanostring technology. These values are compared to similar quantifications in HBV-infected HepG2-hNTCP-A3 target cells at day 7 post-infection.

Figure 7: Cytosolic to nuclear re-localization of HBcAg does not alter HBc18-27 epitope presentation

(a) Cytoplasmic distribution of HBsAg at days 7 and 28 post infection in HepG2-hNTCP-A3 cells using confocal laser scanning microscopy. The HBsAg is stained in green using anti-HBs antibody while the nucleus is stained blue using DAPI.

(b) HBcAg re-localization from cytosolic (days 7 and 14 post-infection) to more nuclear localization (21 and 28 days post-infection) during HBV infection in HepG2-hNTCP-A3 using confocal laser scanning microscopy. HBV-infected HepG2-hNTCP-A3 are stained with anti-HBc antibody (red) and DAPI to stain nucleus (blue).

(c) Ability of CD8+ T cells specific for HBc18-27 to recognize HepG2-hNTCP-A3 infected with HBV for the indicated time. Shown is the frequency of the CD8+ T cells

positive for CD107a among total CD8+ T cells upon co-culture with HepG2-hNTCP-A3 targets for 5 hours at E:T ratio of 1:2. Data are shown as mean ± SD of at least two independent experiments.

(d) Direct quantification of A2-HBc18 complexes on the surface of HBV-infected HepG2-hNTCP-A3 kept in culture for prolonged infection duration. Bars represent the MFI of A2-HBc18 on HBV-infected HepG2-hNTCP-A3 cells normalized to un-infected cells at each time post-infection. MFI is measured using Image Stream analyser.

Table1: Virological and clinical characteristics of CHB patient liver biopsies

Biopsy	HBV Genotype	HLA Typing	HBsAg	HBeAg	TCRl-mAb-Apc
1 (Fig1a,b)	D	A*02:01	POS	POS	POS
2 (Fig 1c,d)	D	A*02:01	POS	POS	POS
3	D	A*02:01	POS	POS	POS
4 (Fig 1e)	C	A*02:01	POS	POS	NEG
5	C	A*02:01	POS	POS	NEG
6	C	A*02:01	POS	POS	NEG
7	B	A*02:01	POS	POS	NEG
8	B	A*02:01	POS	POS	NEG

836
837
838
839
840
841
842
843
844

845 **Table 2: List of cell lines used in experimental systems**

Cell line	Description
HepG2	HLA-A*02:01+, HCC line with no HBV DNA integration
HepG2-hNTCP-A3 (A3 clone)	HepG2 cells overexpressing HBV entry receptor (hNTCP) (14)
HepG2.2.15	HepG2 cells with full HBV genome integration producing virions (10)
HepG2-Env	HepG2 cells transduced with HBV Env (35)
PLC/PRF5- HLA-A*02:01	Natural HCC line with partial HBV surface antigen DNA integration(36) / transduced with HLA-A*02:01 molecule
EBV core	HLA-A*02:01+, EBV immortalized B cell lines transduced with HBV core DNA (8)
HepAD38	HepG2 cells with full HBV genome integration producing virion (41)

846

847

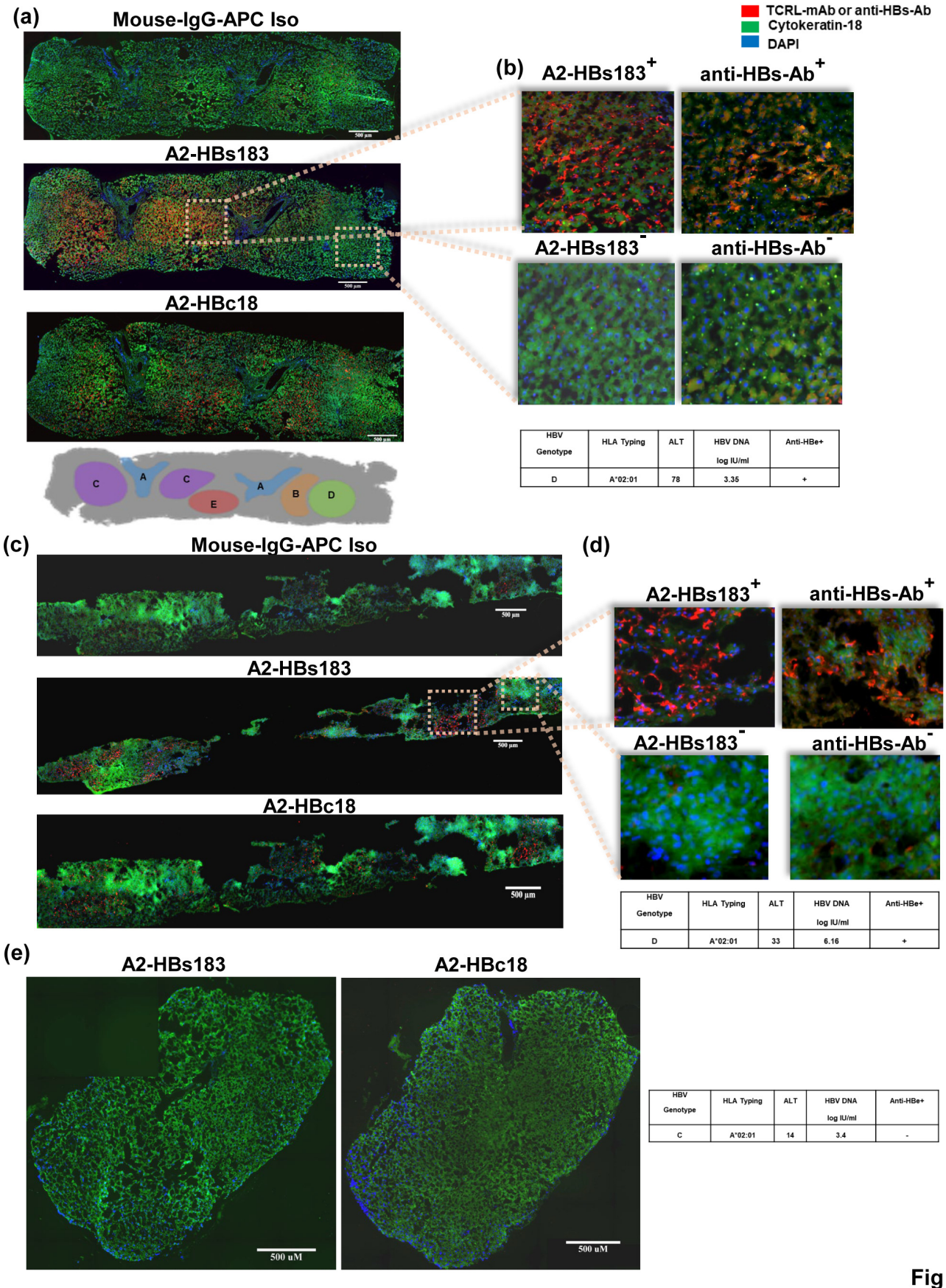

Fig 1

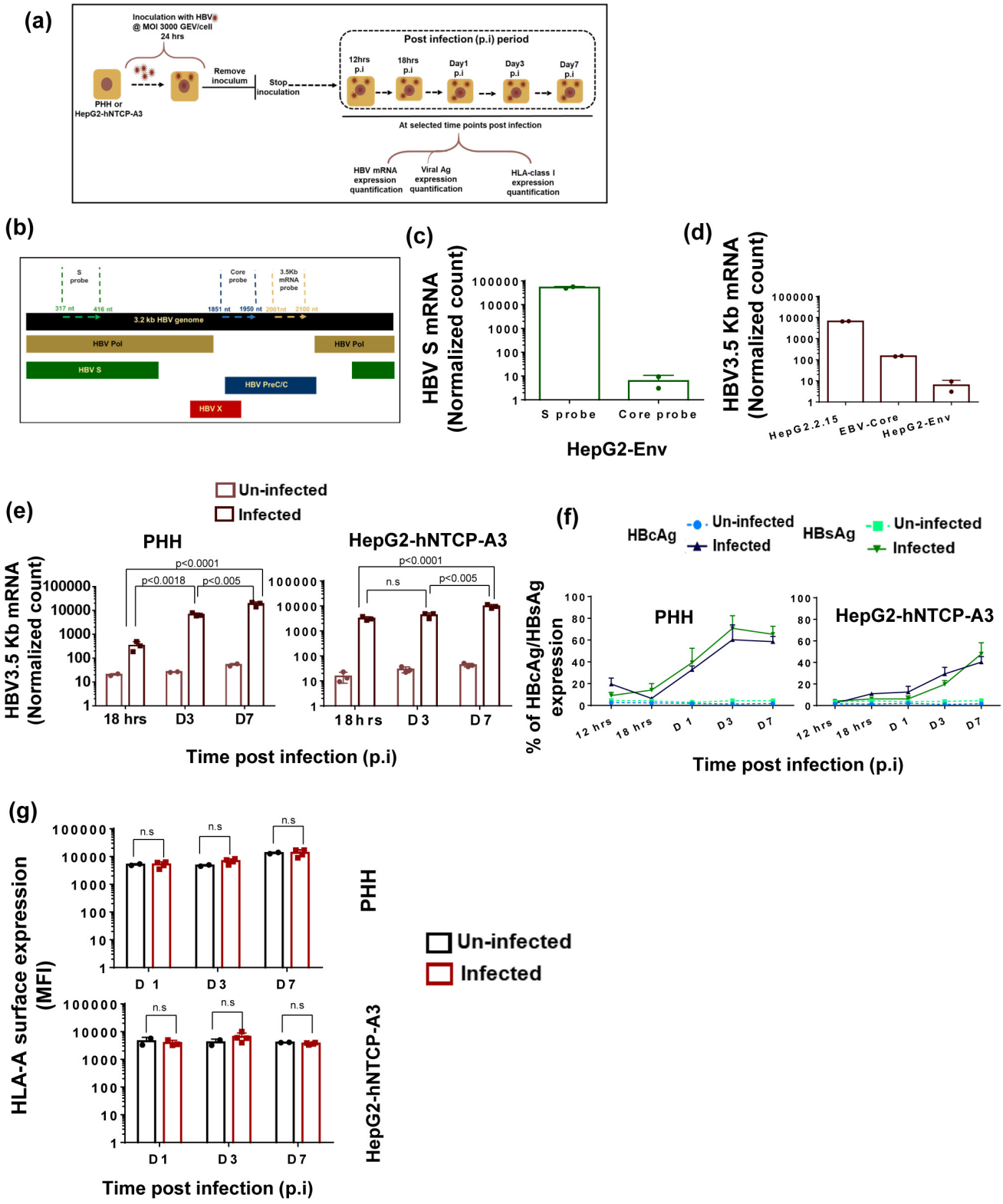

Fig 2

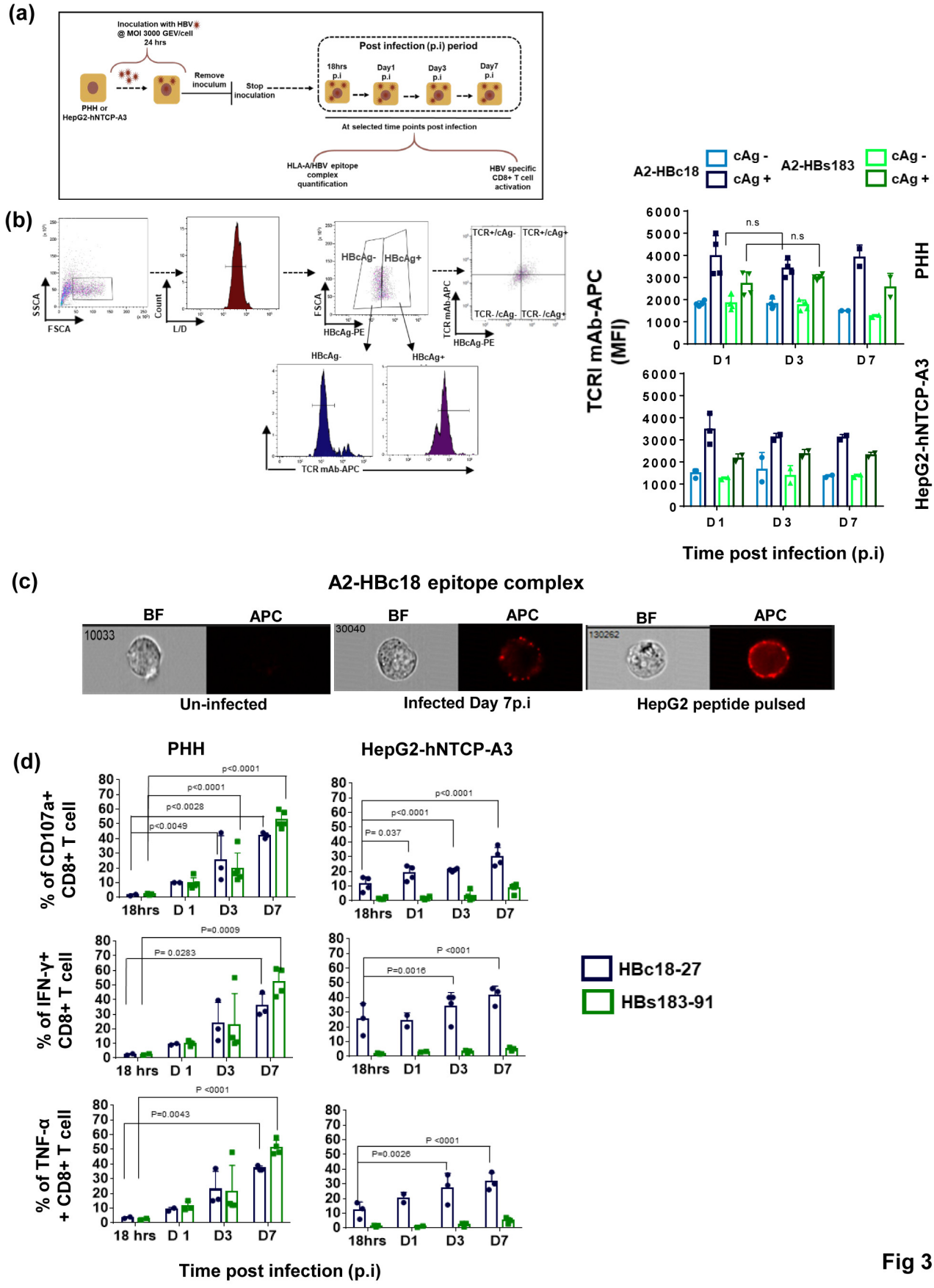

Fig 3

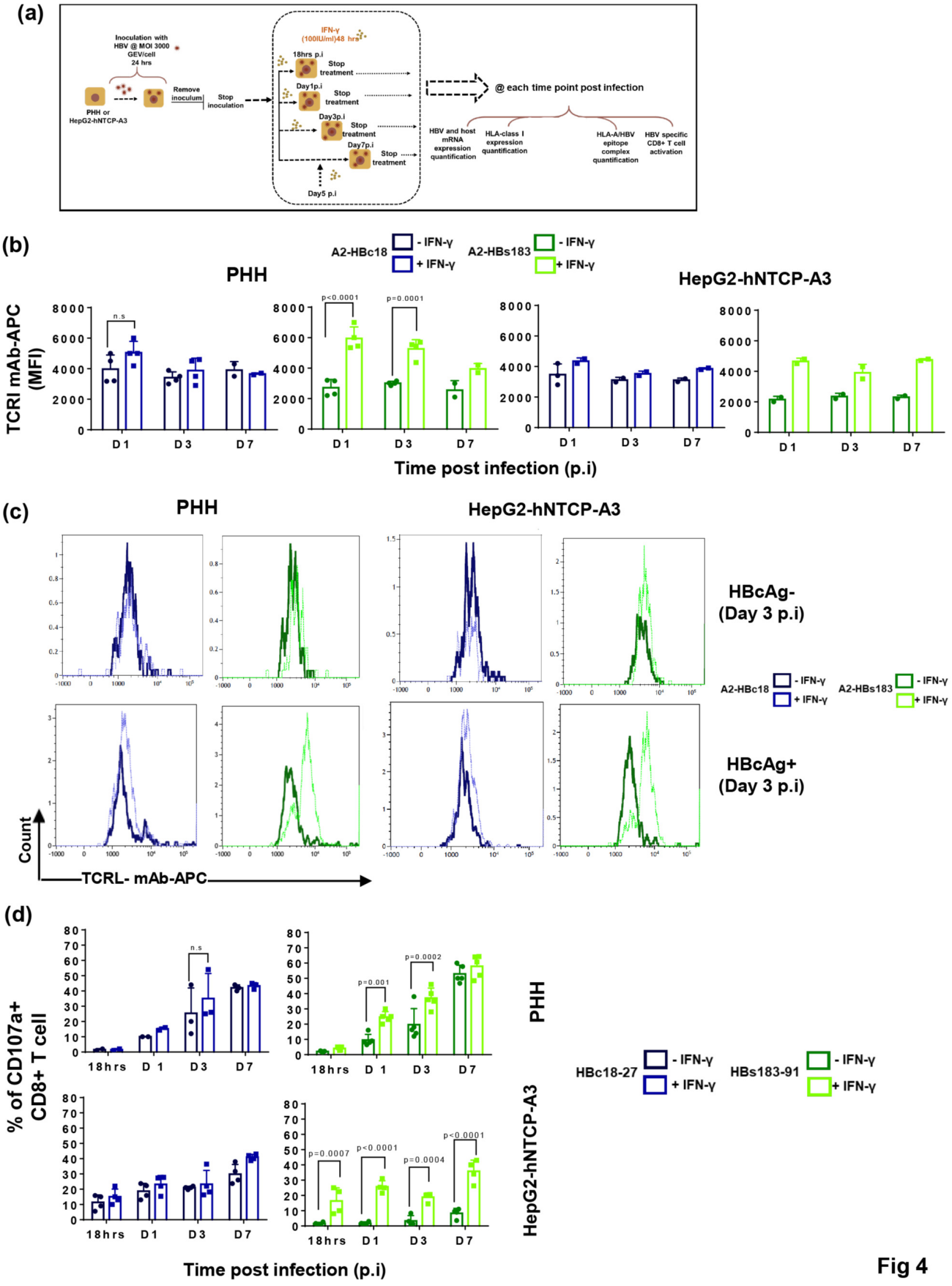

Fig 4

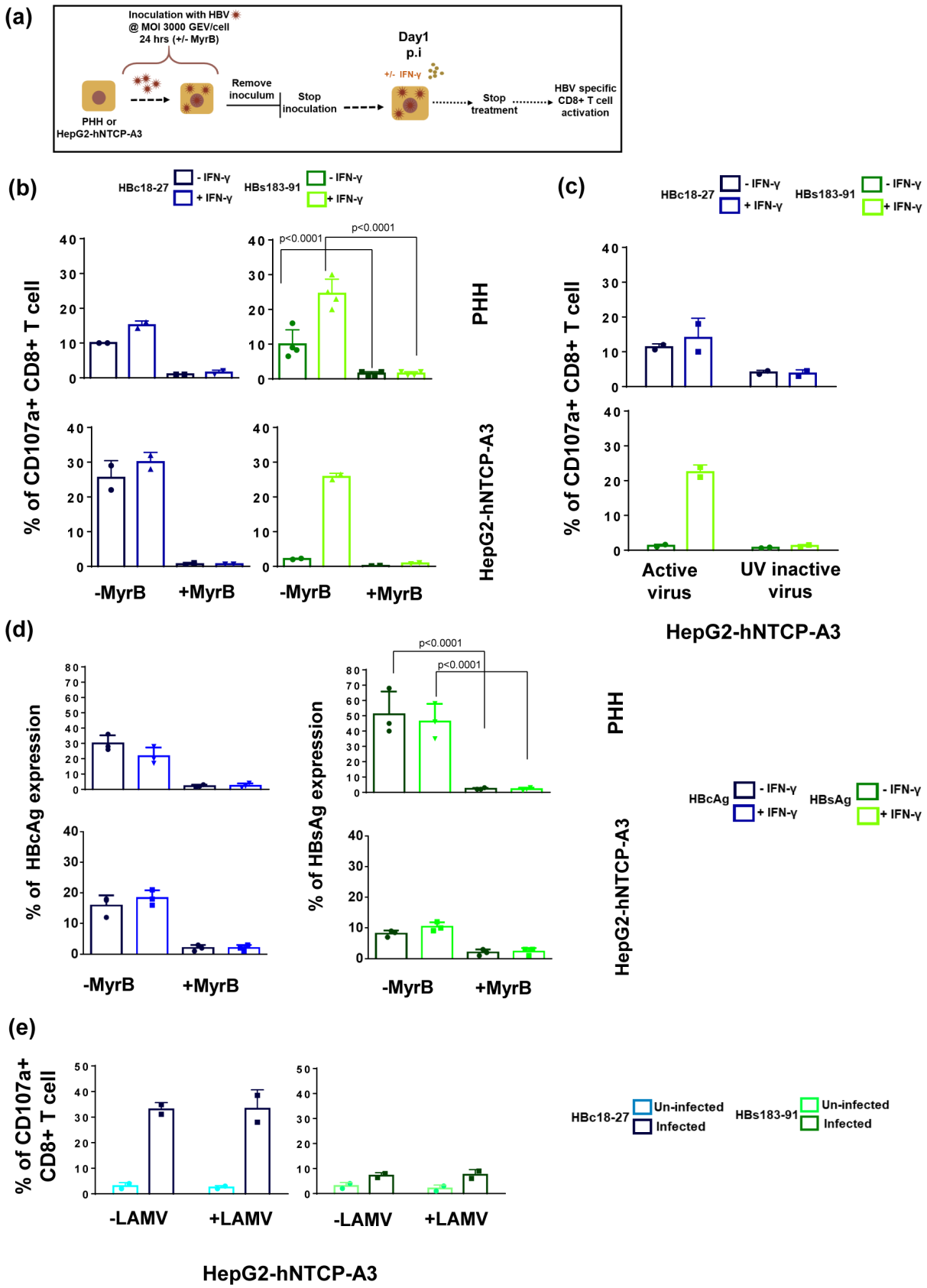

Fig 5

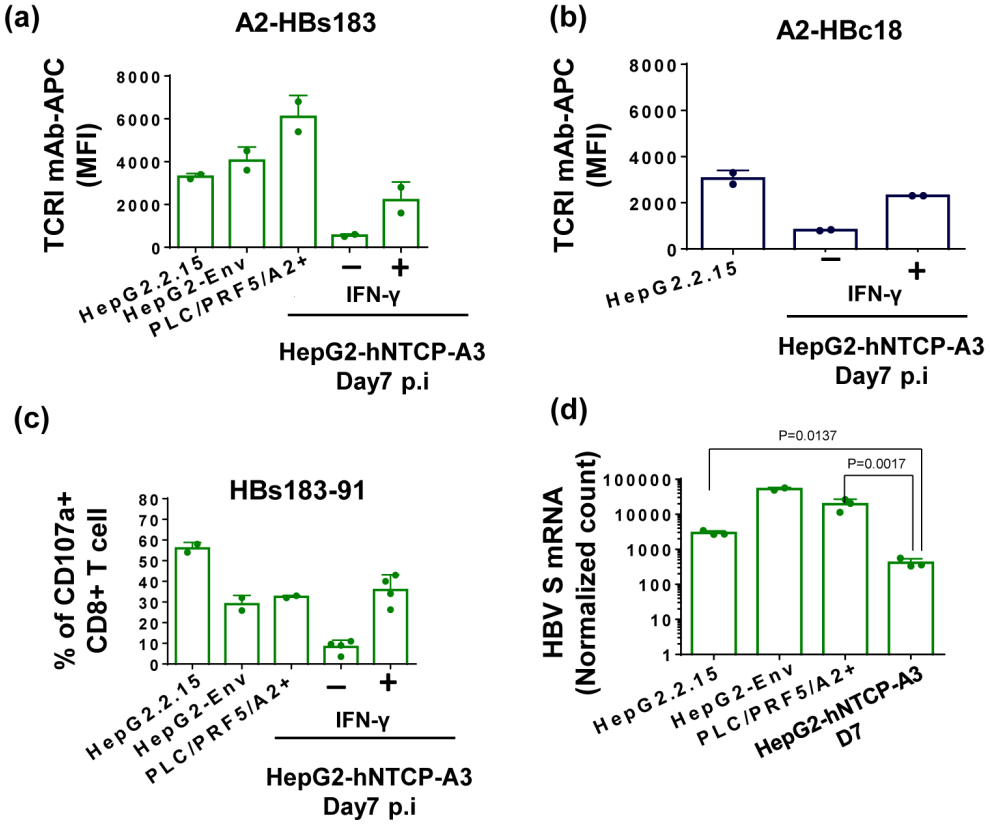

Fig 6

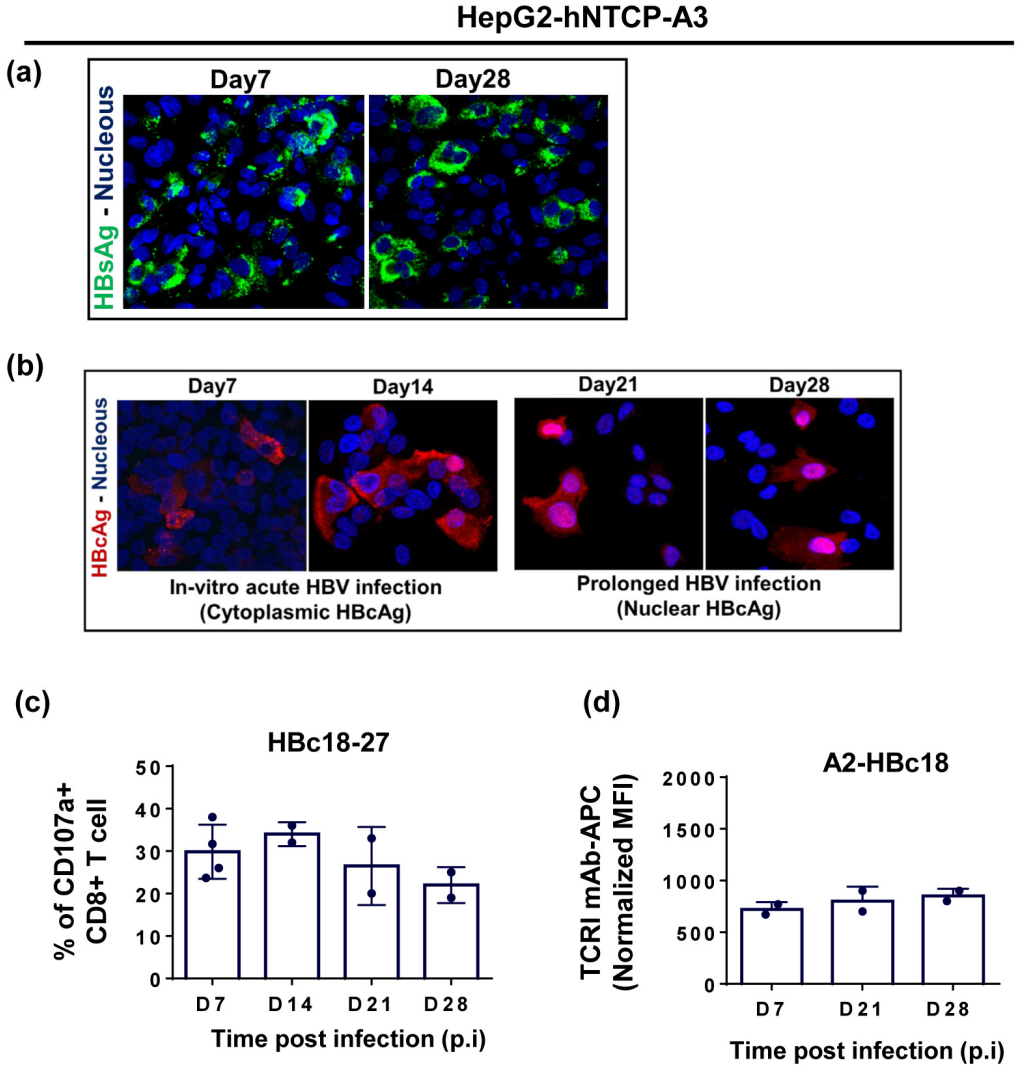

Fig 7